Energy transfer of surface wind induced currents to the deep ocean via resonance with the Coriolis force

Yosef Ashkenazy[1]

[1]*Department of Solar Energy and Environmental Physics, Blaustein Institutes for Desert Research, Ben-Gurion University of the Negev, Sede Boqer Campus 84990, Israel*

(Dated: August 27, 2015)

There are two main comparable sources of the energy to the deep ocean—winds and tides. However, the most efficient mechanism that transfers wind energy to the deep ocean is still debated. Here we show, using oceanic General Circulation Model (GCM) simulations and analytic derivations, that the wind directly supply energy down to the bottom of the ocean when it is stochastic and temporally correlated or when it is periodic with a frequency that matches the Coriolis frequency. Basically, under such, commonly observed, conditions one of the wind components resonates with the Coriolis frequency. Using reanalysis surface wind data and our simple model we show that about one third of the kinetic energy that is associated with wind-induced currents originates from the abyssal ocean, highlighting the importance of the resonance of the wind with the Coriolis force.

PACS numbers: 92.10.A-, 92.10.Ei, 92.60.Gn, 92.60.Cc

Deep ocean mixing is an essential process that maintains the deep ocean circulation—without it the abyssal ocean would have been stagnant [1–3]. Differential heating is insufficient to maintain a closed and steady ocean circulation as the oceanic heat source is on average above the cooling source [3–6]. There are two main comparable sources of deep ocean energy, winds and tides [2]. These increase the vertical mixing by several orders of magnitudes, maintaining the meridional overturning circulation. Ocean circulation would have been restricted to the upper few meters of the ocean if only molecular diffusion was taken into account [2]. There are additional sources of energy to the deep ocean including bottom geothermal heating [6] and biomixing [7]. The common feature for the different energy sources of the abyssal ocean is the large uncertainties associated with them [2].

According to the seminal paper of Ekman [8] wind induced currents are restricted to the upper ocean (first hundred meters or so) and decay exponentially with depth. However, this model is based on the simplistic assumption that the winds are constant, both in space and time. In fact, winds are stochastic by nature and vary on a wide range of temporal and spatial scales. They can generate internal waves, instabilities, and eddies, that eventually radiate into the abyssal ocean; interaction of bottom topography with ocean circulation and eddies also contribute to ocean mixing [2]. Thus, although the Ekman layer model provides the basic understanding on the effect of the Coriolis force on surface currents, it is clear that additional processes that are related to the wind have to be taken into account.

Winds are sometimes periodic. As such, when their frequency matches the inertial (Coriolis) frequency, they can resonate with the currents induced by them. This scenario was discussed in many previous studies [9–15], mainly in the framework of the depth integrated Ekman layer model. Resonance conditions are satisfied when the winds at 30° latitude have diurnal frequency, when the characteristic frequency of a storm matches the Coriolis frequency, or when the tides' frequency matches the Coriolis frequency. In addition, stochastic wind that has temporal correlations can lead to enhanced currents, depending on the strength of the correlation [13, 16, 17]. Here we investigate the effect of the resonance of the wind with the Coriolis force on ocean currents and, in particular, on the abyssal ocean kinetic energy (KE). We carry out oceanic General Circulation Model (GCM) simulations and provide analytic solutions and approximations for the currents as a function of depth for a finite depth ocean under the action of periodic and stochastic wind that exhibits temporal correlations. We show that in both cases the wind induced currents are significant in the deep ocean and contribute significant KE to the abyssal ocean.

We use the MITgcm [18] to study effect of surface winds on ocean current; for more details see the Supplementary Material. We first consider the case of a "box-like" basin with a flat bottom at depth of 1.2 km and constant density. The water surface is forced by a periodic wind stress in the x-direction—the wind's frequency exactly matches the Coriolis frequency such that resonance between the Coriolis force and the wind-stress is expected. The simulation is initiated from a motionless water. The KE as a function of time is presented in Fig. 1a. Two cases are considered—simulation with and without the advection terms. Without the advection terms the equations of motion are linear and eddies cannot be developed while when the advection terms the dynamics is nonlinear and eddies can be developed. At the beginning of the simulation the KE increases monotonically with time (Fig. 1a), the currents are limited to the top ∼100 m of the water column (Fig. 1b) and become strong and almost uniform with time (Fig. 1c). At $t \sim 20$ days the nonlinear advection terms become domi-

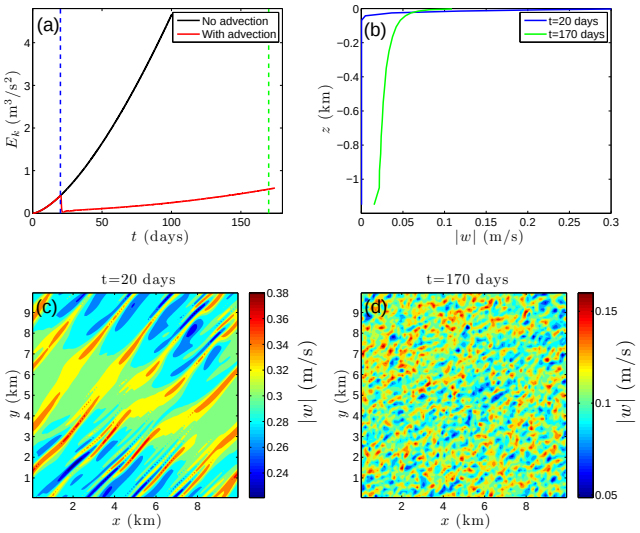

FIG. 1: (a) Depth integrated KE, $\frac{1}{2}\int_H^0 |w|^2 dz$, as a function of time, without (black curve) and with (red curve) the nonlinear advection terms. Note the "collapse" of the KE at $t \approx 21$ days for the run with the advection terms; this collapse is associated with the transition from non-turbulent surface-limited flow to turbulent flow along the entire depth. (b) Current speed as a function of depth just before (blue curve) and after (green curve) the transition shown in the red curve in panel (a). (c) Surface current speed just before the transition—note the almost regular and relatively uniform pattern. (d) Surface current speed after the transition—note the much smaller speed and the turbulent flow pattern.

nant and lead to the development of edge waves (Fig. 1c) [19] and eddies (Fig. 1d) which mix the entire water column and lead an almost uniform speed with depth. This transition is associated with a drastic drop in the KE since the energy is spread over the entire water column, leading to a reduced mean current speed, and thus to reduced KE (as the KE is proportional to the square of the current speed). When the advection terms are excluded (black curve of Fig. 1a) the KE keep increasing to unrealistic values. Repeating the above numerical experiment when the forcing frequency is not equal to the Coriolis frequency, resulted in a much weaker flow that is limited to the upper ∼100 m of the water column. Still, also in this case, at the beginning of the simulation the flow was spatially uniform and was limited to the upper 10-20 m of the water column. Then, after a few days of simulation turbulent flow developed, the upper dynamical layer was deepen to ∼ 100 m, and the current speed reduced. The surface (Ekman-like) layer of the run without the advection terms was deepen monotonically with time until it reached the bottom. The numerical experiments described above indicate that when the forcing frequency matches the Coriolis frequency a resonance occurs resulting in "Ekman" layer that span the entire water column and the mean KE and the current speed are high.

After sufficiently long time the simulated currents are almost uniform in the horizontal directions, in both the barotropic (constant density) and stratified water column cases; see the Supplementary Material. We thus assume in the following that the current's components (u, v) very weakly depend on the horizontal dimensions (x, y) such that it is possible to neglect the advection terms and the horizontal viscosity terms from the governing equations. Then one is left with Ekman model [8]

$$u_t - fv = \nu u_{zz}, \tag{1}$$
$$v_t + fu = \nu v_{zz}, \tag{2}$$

where t and z are the time and depth coordinates, f is the (constant) Coriolis frequency, and ν is the parameterized vertical eddy viscosity coefficient. It is possible to obtain a single equation $w_t + ifw = \nu w_{zz}$, using a complex velocity variable, $w = u + iv$; we then apply a (time) Fourier Transform (FT) to obtain an equation with respect to the depth variable z:

$$\hat{w}_{zz} - i(f+\omega)\hat{w}/\nu = 0, \tag{3}$$

where ω is the frequency variable and the "hat" indicates the FT.

To close the solution of Eq. (3) we apply no-slip boundary conditions at the bottom of the ocean, $\hat{w}(z=-H) = 0$, and at the surface we link the wind stress $\tau = \tau_x + i\tau_y$ (τ_x, τ_y are the x, y components of the wind-stress vector) to the surface currents by $\hat{w}_z(z=0) = \hat{\tau}/(\rho_0\nu)$ [20], where ρ_0 is the ocean water density. The solution is then

$$\hat{w} = \frac{\hat{\tau}(1-i)d}{2\rho_0\nu}\frac{e^{(1+i)(z+H)/d} - e^{-(1+i)(z+H)/d}}{e^{(1+i)H/d} + e^{-(1+i)H/d}}, \tag{4}$$

where $d = \sqrt{2\nu/|f+\omega|}$ is the "spectral" Ekman layer depth.

The FT of the second moment of the currents is given by

$$|\hat{w}|^2 = \frac{|\hat{\tau}|^2 d^2}{2\rho_0^2\nu^2}\frac{\cosh\left[\frac{2(z+H)}{d}\right] - \cos\left[\frac{2(z+H)}{d}\right]}{\cosh\left[\frac{2H}{d}\right] + \cos\left[\frac{2H}{d}\right]}. \tag{5}$$

The frequency spectrum of the KE per unit area is then

$$\hat{E}_k = \frac{1}{2}\int_{-H}^{0} |\hat{w}|^2 dz = \frac{|\hat{\tau}|^2 d^3}{8\rho_0^2\nu^2}\frac{\sinh\left(\frac{2H}{d}\right) - \sin\left(\frac{2H}{d}\right)}{\cosh\left(\frac{2H}{d}\right) + \cos\left(\frac{2H}{d}\right)}. \tag{6}$$

The depth of the Ekman layer, d, diverges when $\omega = -f$ and the wind-induces currents may reach the bottom of the ocean, depending on the frequency spectrum of the wind stress, $\hat{\tau}$.

To explicitly find the currents there is a need to know the wind-stress and to apply an inverse FT or to use the Parseval's theorem, i.e.,

$$\langle |w|^2 \rangle = \frac{1}{2\pi}\int_{-\infty}^{\infty} |\hat{w}|^2 d\omega. \tag{7}$$

Below we consider two cases: (i) a purely periodic wind stress, and (ii) stochastic wind stress with temporally decaying correlations.

Periodic wind stress. For simplicity we choose the wind stress to be periodic only in the x direction such that $\tau(t) = \tau_{x,0}\cos(\omega_0 t)$ where $\tau_{x,0}$ is the wind-stress amplitude in the x directions and ω_0 is the frequency; below, for convenience, we drop the subscript x. The FT of the wind stress is then a sum of two δ functions and hence

$$w(t) = \frac{\sqrt{2}\tau_0}{4\rho_0\nu}\sum_{j=+,-} d(j\omega_0)\frac{\sinh\left[\frac{(1+i)(z+H)}{d(j\omega_0)}\right]}{\cosh\left[\frac{(1+i)H}{d(j\omega_0)}\right]}e^{i(j\omega_0 t-\frac{\pi}{4})}. \tag{8}$$

The second moment of the currents is then

$$\langle w^2\rangle = \frac{\tau_0^2}{8\rho_0^2\nu^2}\sum_{j=+,-}[d(j\omega_0)]^2\frac{\cosh\left[\frac{2(z+H)}{d(j\omega_0)}\right]-\cos\left[\frac{2(z+H)}{d(j\omega_0)}\right]}{\cosh\left[\frac{2H}{d(j\omega_0)}\right]+\cos\left[\frac{2H}{d(j\omega_0)}\right]}, \tag{9}$$

and the KE is

$$E_k = \frac{\tau_0^2}{32\rho_0^2\nu^2}\sum_{j=+,-}[d(j\omega_0)]^3\frac{\sinh\left[\frac{2H}{d(j\omega_0)}\right]-\sin\left[\frac{2H}{d(j\omega_0)}\right]}{\cosh\left[\frac{2H}{d(j\omega_0)}\right]+\cos\left[\frac{2H}{d(j\omega_0)}\right]}. \tag{10}$$

Generally speaking, the depth of the Ekman layer, d, is much smaller than the depth of the ocean, H. In this case the currents decay exponentially with depth and Eqs. (8)-(10) become independent of the ocean depth H; the current vector exhibits periodic clockwise rotation with frequency ω_0.

In the case of "resonance" the wind-stress frequency equals the Coriolis frequency ($\omega_0 = f$) and the depth of the Ekman layer becomes infinite, and hence much larger than the depth of the ocean. Then, based on Eq. (8) the current vector may be approximated as

$$[u(t), v(t)] = (z+H)\tau_0[\cos(ft), -\sin(ft)]/(2\rho_0\nu) \tag{11}$$

Consequently the current's second moment and KE are

$$|w|^2 = \frac{\tau_0^2}{4\rho_0^2\nu^2}(z+H)^2 \tag{12}$$

$$E_k = \frac{\tau_0^2}{24\rho_0^2\nu^2}H^3. \tag{13}$$

Hence, under resonance conditions: (i) the current's magnitude depends on the depth of the ocean and decreases linearly with depth to the bottom of the ocean, (ii) the current vector rotates clockwise with the Coriolis frequency, with a fixed magnitude, and (iii) the KE increases like H^3.

We validate the analytic solutions given above by comparing them with the MITgcm simulations. In these simulations we focus on resonance conditions, excluding the spatial dependence. The results are shown on the left column of Fig. 2. The analytic solutions (black lines) are very close to the numerical ones (blue full circles), including (i) the clockwise rotation of the current vector with the Coriolis frequency (not shown), (ii) the linear decrease of the current speed with depth z (Fig. 2a), (iii) the linear increase of surface current speed with the depth of the ocean, H (Fig. 2c), and (iv) the cubic dependence of the KE on the depth of the ocean, H (Fig. 2e). Under non-resonance conditions the currents are limited to the surface Ekman layer and are independent of the depth of the ocean. The small deviations between the analytic expressions and the numerical results may be attributed, in part, to the additional bottom linear friction of the MITgcm. It is important to note that when the current's components u and v depend linearly on depth z, the viscosity terms in Eqs. (1),(2) vanish such that the equations take the form of the equations associated with inertial oscillations that exhibit clockwise rotation of the current vector with the Coriolis frequency.

Resonance of the Coriolis force with other driving forces like diurnal winds or tides is limited to a very narrow band of latitudes, questioning the overall effect of the resonance on real ocean circulation and energy. However, winds are stochastic in their nature such that one components of their frequency spectrum may resonate with the Coriolis force across the globe. This may lead to an enhancement of wind induced currents over wide regions, possibly penetrating to the bottom of the ocean. Next we study this hypothesis.

Stochastic wind stress. To study the effect of stochastic wind on ocean currents, we forced the model with a stochastic wind that its temporal correlations decay exponentially,

$$\langle\tau(\tilde{t})\tau(\tilde{t}+t)\rangle = \frac{\tau_0^2}{2}e^{-\gamma|t|} \tag{14}$$

where τ_0 is a parameter that quantifies the magnitude of the wind stress and γ is a parameter that quantifies the decay rate of the temporal correlations; see also [17, 21]. Similar to the above, for simplicity we restrict the winds to be along the x direction. The FT of the wind stress (14) is

$$|\hat{\tau}|^2 = \frac{\gamma\tau_0^2}{\gamma^2+\omega^2}. \tag{15}$$

We first use this wind stress to simulate currents using the MITgcm. The configuration is the same as the one presented above, i.e., a domain of 100×100 horizontal grid points with resolution of 100 m and a 1.2 km deep ocean, with doubly periodic boundary conditions. This configuration and forcing resulted in spatially, almost uniform, currents. We thus use the spatially independent Eqs. (1),(2) and the solution (5) to gain more understanding on the system's dynamics. We develop

in the Supplementary Material analytic approximations for the dependence of the second moments of the current speed $|w|^2$ on depth z, for the dependence of the surface current speed on ocean depth H, and for the dependence of the KE on ocean depth, $E_k(H)$.

We show that when the wind stress is stochastic with exponentially decaying temporal correlations, the current speed is not limited to the upper ocean but decreases linearly in the lower part of the ocean and vanishes only at the ocean floor; see Fig. 2b and Eq. (S10). This is due to the "resonance"-like of the Coriolis force with the wind stress at the Coriolis frequency. At this frequency the Ekman layer becomes infinite, leading to the penetration of wind induced currents to the bottom of the ocean. The decrease is faster at the upper part of the ocean [Fig. 2b and Eqs. (S11),(S12)]. The MITgcm simulations exhibit similar decrease with depth (full circles in Fig. 2b).

The second moment of the surface current speed, $|w|^2$ as a function ocean depth, H, is shown in Fig. 2d. The analytic approximation (S13) indicates a logarithmic increase of $|w|^2$ with H and is in good agreement with the MITgcm simulations (Fig. 2d). The analytic approximation of the KE, Eq. (S17), points to a linear increase with the ocean depth, H. The agreement with the MITgcm simulations is satisfactory and better for shallower depths (Fig. 2f). In summary, under the action of temporally correlated stochastic wind stress, the currents are not confined in the upper ocean as in the classical Ekman layer model, but extend to the bottom of the ocean.

As the wind is stochastic and exhibits temporal correlations [17] the resonance of stochastic wind-stress with the Coriolis force is relevant everywhere on the globe. Our calculations (see Supplementary Material) indicate that the contribution of the stochastic wind stress is relevant in vast ocean regions and is much larger than the periodic wind stress component that is restricted to the latitude 30°. In addition, 34% of the energy due to the resonance of the Coriolis force with the stochastic part of the wind is absorbed in the deep ocean (deeper than 1 km). The contribution associated with the mean wind stress is much smaller than the contribution due to the stochastic and periodic parts of the wind stress, and is negligible in the deep ocean. While these estimations are based on realistic wind stress, they are very rough due to the simplistic assumptions of our approach, in particular due to the choice of the eddy parameterized viscosity coefficient, ν, which depends on the eddy activity. Yet, our results highlight the possible importance of the temporal variability of the wind on the transformation of wind KE to the deep ocean.

In summary, we study the role of the variability of the wind on deep ocean currents. We first show, using the MITgcm, that when the wind is periodic with a frequency that matches the Coriolis frequency and when starting from rest, turbulent flow is developed that eventually lead to the mixing of the entire water column and to a constant interior ocean current speed. Under stratification conditions imposed at the sides of the domain, the current speed decreases linearly with depth z and vanishes only at the bottom of the ocean. In all cases the current field is almost laterally uniform, justifying the omission of the advection and lateral viscosity terms. We then provide an analytic solution for the currents under the action of periodic wind stress and find that the current speed decreases linearly with depth z and only vanishes at the ocean floor. The surface current speed depends linearly on the ocean depth and the KE increases as a function of the cube of the ocean depth H. Under more realistic stochastic and temporally correlated wind stress, one of the wind's frequencies resonates with the Coriolis force, causing the currents to reach the bottom of the ocean. We show, numerically and via analytic approximations, that the current speed in the deep ocean decreases linearly with depth z, that the second moment of the surface current increases logarithmically with the ocean depth H, and that the KE increases linearly as a function of ocean depth H. Thus, when considering the infinite depth Ekman layer model an additional friction term has to be included to avoid the singularity of the ocean currents [21, 24].

Under realistic global ocean bathymetry and realistic wind stress forcing the contribution of the stochastic component of the wind stress is much larger than the contribution of the periodic component of the wind stress and the (temporal) mean wind stress, which is negligible. The stochastic component of the wind stress is significant in extended ocean areas, unlike the periodic component which is significant only at 30° latitude, where the Coriolis force resonates with the diurnal winds. Moreover, around one third of the KE is stored in ocean depths deeper than 1 km. While this a very rough estimate due to the simplicity of the model it indicates that the stochastic nature of the wind has an important role in the energy budget of the deep ocean.

We thank Golan Bel, Georgy Burde, Hezi Gildor, Avi Gozolichiani, and Eli Tziperman for helpful discussions.

[1] W. Munk, Deep Sea Res. **13**, 707 (1966).
[2] W. Munk and C. Wunsch, Deep Sea Res. **45**, 1977 (1998).
[3] C. Wunsch and R. Ferrari, Ann. Rev. Fluid Mech. **36**, 281 (2004).
[4] J. W. Sandström, Annalen der Hydrographie under Martimen Meteorologie **36**, 6 (1908).
[5] A. Defant, (1961).
[6] R. X. Huang, J. Phys. Oceanogr. **29**, 727 (1999).
[7] W. K. Dewar, R. J. Bingham, R. Iverson, D. P. Nowacek, L. C. St Laurent, and P. H. Wiebe, Journal of Marine Research **64**, 541 (2006).
[8] V. W. Ekman, Arch. Math. Astron. Phys. **2**, 1 (1905).
[9] D. L. Rudnick and A. Weller, R., J. Phys. Oceanogr. **23**, 2359 (1993).

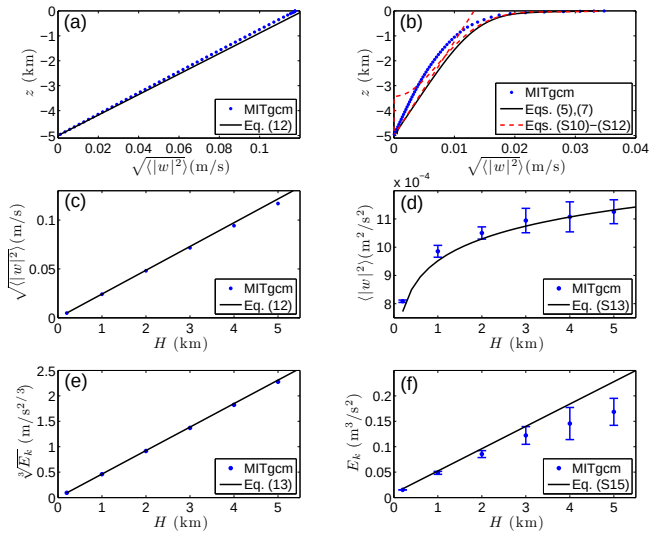

FIG. 2: Summary of the MITgcm 1d simulation for periodic wind-stress forcing under resonance condition with the Coriolis frequency (left column) and stochastic, temporally correlated, wind stress (right column). (a) Current speed as a function of depth z under the action of periodic wind stress. (b) Same as (a) for (stochastic) correlated wind stress; note that the analytic approximations fall within the error-bars of the simulations (not shown). (c) Surface current speed as a function of ocean depth, H, when the wind stress is periodic. (d) Same as (c) for for (stochastic) correlated wind stress. (e) Depth integrated KE, $E_k^{3/2}$, as a function of ocean depth, H, under the action of periodic wind stress. (f) Same as (e) for stochastic and temporally correlated wind-stress. In all panels the MITgcm simulation are indicated by the blue dots while the analytic solutions/ approximations are indicated by the solid and dashed lines. The error bars indicate mean $\pm$ 1 standard deviation of 20 MITgcm realizations. Parameter values: $\tau_0 = 0.005$ (0.1) N m^{-2} for periodic (stochastic) wind stress, ρ_0=1028 kg m^{-3}, $\nu = 0.1$ m^2 s^{-1}, $\gamma = 10^{-5}$ s^{-1}, and $\omega_0 = f = 2\pi/86400$ s^{-1}.

[10] G. B. Crawford and W. G. Large, J. Phys. Oceanogr. **26**, 873891 (1996).

[11] D. L. Rudnick, in *Near-Boundary Processes and Their Parameterization, Proceedings of the 13th 'Aha Huliko'a Hawaiian Winter Workshop*, edited by P. Müller and D. Henderson (University of Hawaii, 2003) pp. 163–170.

[12] R. G. Stockwell, W. G. Large, and R. F. Milliff, Tellus A **56**, 536547 (2004).

[13] J. C. McWilliams and E. Huckle, J. Phys. Oceanogr. **36**, 1646 (2005).

[14] J. B. Mickett, Y. L. Serra, M. F. Cronin, and M. H. Alford, J. Phys. Oceanogr. **40**, 401 (2010).

[15] D. B. Whitt and L. N. Thomas, J. Phys. Oceanogr. **45**, 181208 (2015).

[16] J. Gonella, Deep Sea Res. **18**, 775 (1971).

[17] G. Bel and Y. Ashkenazy, New J. Phys. **15**, 053024 (2013).

[18] MITgcm-group, *MITgcm User Manual*, Online documentation (MIT/EAPS, Cambridge, MA 02139, USA, 2010) http://mitgcm.org/public/r2_manual/latest/online_documents/n

[19] G. K. Vallis, *Atmospheric and Oceanic Fluid Dynamics* (Cambridge University Press, Cambridge, U.K., 2006) p. 745.

[20] A. E. Gill, *Atmosphere–ocean dynamics* (Academic Press, London, 1982) p. 662.

[21] Y. Ashkenazy, H. Gildor, and G. Bel, Europhysics Lett. **accepted** (2015).

[22] A. Gargett, J. Mar. Res. **42**, 359 (1984).

[23] W. G. Large, J. C. Mcwilliams, and S. C. Doney, Rev. Geophys. **32**, 363 (1994).

[24] S. Y. Kim, P. M. Kosro, and A. L. Kurapov, J. Geophys. Res. **119**, 6631 (2014).

[25] M. Kanamitsu, W. Ebisuzaki, J. Woollen, S.-K. Yang, J. Hnilo, M. Fiorino, and G. Potter, Bulletin of the American Meteorological Society **83**, 1631 (2002).

[26] W. G. Large and S. G. Yeager, *Diurnal to decadal global forcing for ocean and sea-ice models: the data sets and flux climatologies* (Citeseer, 2004).

[27] J. S. vonStorch, C. Eden, I. Fast, H. Haak, D. Hernández-Deckers, E. Maier-Reimer, J. Marotzke, and D. Stammer, J. Phys. Oceanogr. **42**, 2185 (2012).

[28] S. E. Levitus, *Climatological atlas of the world ocean* (NOAA Professional Paper 13, US Government Printing Office, Washington DC, 1982) p. 173.

Supplemental Material: Energy transfer of surface wind induced currents to the deep ocean via resonance with the Coriolis force

MITgcm SETUP AND SIMULATIONS

We use the Massachusetts Institute of Technology general circulation model [MITgcm, S18] to study oceanic circulation under the action of periodic and stochastic wind stress. We use a simple rectangular domain with doubly periodic boundary conditions in the lateral x and y directions and with bottom no-slip (zero velocity) boundary conditions. The ocean floor is flat. The horizontal grid resolution is 100 m, the vertical grid resolution increased monotonically from 4 m at top layer to 100 m at depth of 200 m; then a constant vertical grid spacing of 100 m was used down to the bottom of the ocean (which is 1.2 km in the main example discussed in the main text). There are 100×100 grid points in the horizontal direction (10×10 km), to both resolve possible eddy activities and to capture possible non-hydrostatic effects. The Coriolis parameter is taken to be constant. The only driving force is the wind stress which is temporally variable but spatially constant. We study the ocean current both when the ocean is stratified and when it had uniform density.

THE ROLE OF DENSITY STRATIFICATION IN THE EFFECT OF RESONANCE

Intuitively, stratification of the water column should limit vertical motion and thus should weaken the effect of the resonance discussed in the main text. When starting the simulation with stratified water column (by initially specifying the water temperature from 20°C at the top to 10°C at the bottom), after some time eddies are developed and erode the stratification such that eventually the entire water column is mixed and has an uniform density. The current speed profile then converges to the almost uniform profile shown in Fig. 1b.

To mimic real ocean stratification we performed an additional simulation in which the temperature at the sides of the box is kept constant, imposing stratification at the boundaries of the box throughout the simulation. The results of this simulation are shown in Fig. S1 where we imposed the linear temperature profile indicated by the red line in Fig. S1c. There are several important observations: (i) variations in sea surface height are small (Fig. S1a), suggesting that the horizontal variations in the current field are small and that eddy activity is weak; (ii) the currents are practically uniform in the horizontal directions (Fig. S1a); (iii) u is perpendicular to v (Fig. S1a,b); (iv) the magnitude of u equals the magnitude of v (Fig. S1a,b); (v) u and v oscillate sinusoidally with time such that the current vector is rotating clockwise with frequency of 1 day (Fig. S1b); (vi) the current speed is almost constant with time; (vii) u and v (and hence the current speed) decrease linearly with depth (Fig. S1c) such that the current vector direction is constant with depth; (viii) the slope of linear decrease of the current speed from (vii) converges to a constant value for sufficiently strong stratification (Fig. S1d).

It is clear that for sufficiently strong imposed stratification, the developed eddies will not be able to break the stratification; we thus expect the slope $|w|_z$ to converge exponentially to a limiting value with the level of stratification T_z. The two limits of this dependence can be deduced from our analysis: when $T_z \to 0$ also $|w|_z \to 0$ (Fig. 1) and when $T_z \to \infty$ Eq. (12) holds and $|w|_z = \frac{\tau_0}{2\rho_0\nu}$. Thus, if $\rho_z = \text{const}$ then

$$|w|_z = \frac{\tau_0}{2\rho_0\nu}\left(1 - e^{\frac{aH}{\rho_0}\rho_z}\right), \tag{S1}$$

where a is a constant that quantifies the decay rate and can be estimated from the simulated currents. It is possible to obtain the interior ocean profile by integrating Eq. (S1)

$$|w(z)| = \frac{\tau_0}{2\rho_0\nu}(z+H) - \frac{\tau_0}{2\rho_0\nu}e^{\frac{aH}{\rho_0}\rho_z}\left(z+H-h_0\right), \tag{S2}$$

where h_0 is an additional constant that can be estimated from the simulations.

TEMPORALLY CORRELATED STOCHASTIC WIND STRESS

Given the FT of the of temporally correlated wind-stress, Eq. (15), it is possible to find the FT of the second moment of the currents, using Eq. (5). The second moment of the currents is obtained by using the Parseval's relation, Eq. (7). Eq. (5) is singular when $\omega = -f$ and the integral (7) around this point can be approximated as

$$I_2 = \frac{\tau_0^2(H+z)^2}{2\pi\rho_0^2\nu^2}\int_{\omega_1}^{\omega_2}\frac{\gamma}{\gamma^2+\omega^2}d\omega. \tag{S3}$$

Far from the point of singularity, Eq. (5) can be approximated as

$$|\hat{\omega}|^2 \approx \frac{|\hat{\tau}|^2}{\rho_0^2\nu}\frac{e^{2z/d}}{|f+\omega|} \approx \frac{|\hat{\tau}|^2}{\rho_0^2\nu}\frac{1}{|f+\omega|}. \tag{S4}$$

Then, when $\omega \ll -f$, integral (7) can be approximated as

$$I_1 = -\frac{\tau_0^2}{2\pi\rho_0^2\nu}\int_{\omega_l}^{\omega_1}\frac{\gamma}{\gamma^2+\omega^2}\frac{1}{f+\omega}d\omega, \tag{S5}$$

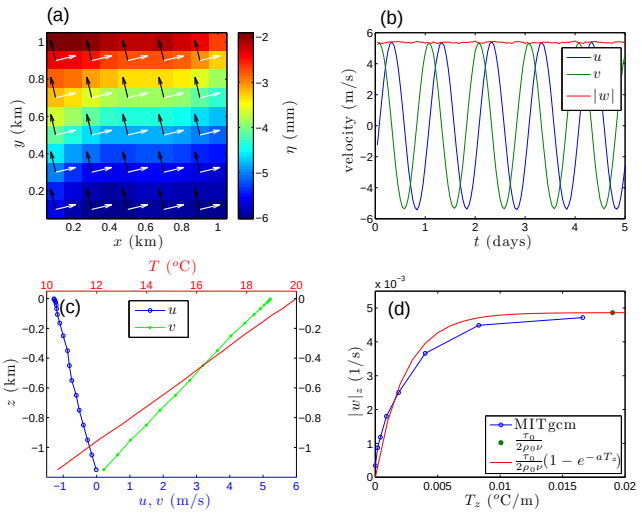

FIG. S1: (a) See surface height (color) and surface velocities u, v (black and white arrows) under stratification conditions. (b) u (blue), v (green) and current speed (red) as a function of time. (c) u (blue open circle), v (blue full circle) as a function of depth under temperature stratification conditions (red curve). (d) Gradient in current speed as a function of stratification temperature gradient for the MITgcm simulations (blue open circles) and for the exponential fit (red curve) similar to Eq. (S1). The green full circle indicates the theoretically predicted current speed, $\tau_0/(2\rho_0\nu)$, under very strong stratification ($T_z \to \infty$). Parameter values: $\tau_0 = 0.1$ N m^{-2}, ρ_0=1028 kg m^{-3}, $\nu = 0.01$ m^2 s^{-1}, $\omega_0 = f = 2\pi/86400$ s^{-1}, and $a = 420$ m K^{-1}.

and when $\omega \gg -f$ it can be approximated as

$$I_3 = \frac{\tau_0^2}{2\pi\rho_0^2\nu}\int_{\omega_2}^{\omega_r}\frac{\gamma}{\gamma^2+\omega^2}\frac{1}{f+\omega}d\omega. \tag{S6}$$

The limits $\omega_{1,2}$ of $I_{1,2,3}$ connect the different regions of the integral and are found based on the numerical results:

$$\omega_{1,2} = \mp\frac{\pi\nu}{H^2} - f. \tag{S7}$$

The limits $\omega_{l,r}$ are found such that the linear approximation of the exponent in Eq. (S4) is zero,

$$\omega_{l,r} = \mp\frac{\nu}{2z^2} - f. \tag{S8}$$

Given the above limits, I_2 is found to be

$$I_2 = \frac{\tau_0^2(H+z)^2}{2\pi\rho_0^2\nu^2}\left[\tan^{-1}\left(\frac{\pi\nu}{\gamma H^2}-\frac{f}{\gamma}\right)+\tan^{-1}\left(\frac{\pi\nu}{\gamma H^2}+\frac{f}{\gamma}\right)\right]. \tag{S9}$$

I_2 can be further approximated as,

$$I_2 \approx \frac{\tau_0^2(H+z)^2}{\rho_0^2\nu}\frac{\gamma}{f^2+\gamma^2}. \tag{S10}$$

We find that I_2 reproduces fairly well the second moment of the current speed close to the bottom.

Close to the surface of the ocean the second moment of the currents can be approximated by I_1+I_3 which can be expressed, given the limits $\omega_{l,1,2,r}$ as follows,

$$\begin{aligned} I_1 &= \frac{\tau_0^2}{4\pi(\gamma^2+f^2)\rho_0^2\nu} \\ &\left[2f\left(\tan^{-1}\left(\frac{\pi\nu}{\gamma H^2}+\frac{f}{\gamma}\right)-\tan^{-1}\left(\frac{\nu}{2\gamma z^2}+\frac{f}{\gamma}\right)\right)+\right. \\ &\left.\gamma\ln\frac{\gamma^2H^4+(\pi\nu+H^2f)^2}{4\pi^2\gamma^2z^4+(\nu+2fz^2)^2}\right] \end{aligned} \tag{S11}$$

$$\begin{aligned} I_3 &= \frac{\tau_0^2}{4\pi(\gamma^2+f^2)\rho_0^2\nu} \\ &\left[2f\left(\tan^{-1}\left(\frac{\nu}{2\gamma z^2}-\frac{f}{\gamma}\right)-\tan^{-1}\left(\frac{\pi\nu}{\gamma H^2}-\frac{f}{\gamma}\right)\right)+\right. \\ &\left.\gamma\ln\frac{\gamma^2H^4+(\pi\nu-H^2f)^2}{4\pi^2\gamma^2z^4+(\nu-2fz^2)^2}\right]. \end{aligned} \tag{S12}$$

Thus, following Eq. (S10), close to the bottom the current speed decreases linearly with depth, z. Simple analysis of I_1+I_3 of Eqs. (S11),(S12) indicates that close to the surface of the ocean the decrease of current speed with depth z is approximately logarithmic.

Based on I_1+I_3 of Eqs. (S11),(S12) we approximate the second moment of the surface current ($z=0$) as

$$\begin{aligned} |w|^2 &\approx \frac{\tau_0^2}{\pi(\gamma^2+f^2)\rho_0^2\nu}\left[f\tan^{-1}\left(\frac{f}{\gamma}\right)+\right. \\ &\left.\gamma\ln\left(\frac{\sqrt{\gamma^2+f^2}}{\nu}\right)+2\gamma\ln H\right]. \end{aligned} \tag{S13}$$

Thus, $|w|^2$ grow logarithmically with the ocean depth, H.

It is possible to approximate the total KE similar to the above treatment. Based on Eq. (6), the FT of the KE close to the singularity point ($\omega = -f$) is approximated as

$$\hat{E}_k \approx \frac{|\hat{\tau}|^2H^3}{6\rho_0^2\nu^2}, \tag{S14}$$

and given Eqs. (15), (7) the KE is then

$$\begin{aligned} E_k &\approx \frac{\tau_0^2H^3}{12\pi\rho_0^2\nu^2}\int_{\omega_1}^{\omega_2}\frac{\gamma}{\omega^2+\gamma^2}d\omega = \\ &\frac{\tau_0^2H^3}{12\pi\rho_0^2\nu^2}\left[\tan^{-1}\left(\frac{3\pi\nu}{2\gamma H^2}-\frac{f}{\gamma}\right)+\tan^{-1}\left(\frac{3\pi\nu}{2\gamma H^2}+\frac{f}{\gamma}\right)\right] \end{aligned} \tag{S15}$$

where the limits $\omega_{1,2}$ are

$$\omega_{1,2} = \mp\frac{3\pi\nu}{2H^2} - f. \tag{S16}$$

As the depth of the ocean is usually much larger than the depth of Ekman layer (i.e., $H^2 \gg \frac{3\pi}{4}\frac{2\nu}{f}$), the KE can be further simplified,

$$E_k \approx \frac{\gamma\tau_0^2}{4\rho_0^2\nu(\gamma^2+f^2)}H. \quad \text{(S17)}$$

Thus, when the wind stress is stochastic with exponentially decaying correlations, the KE increases linearly on the depth of the ocean H.

IMPLEMENTATION TO THE REAL OCEAN

To get a rough idea on the effect of the resonance on the real ocean, we used the six-hourly winds of NCEP-DOE reanalysis 2 [S25]. Global coverage ($\sim$2.5°) surface (10 m) winds of 36 years (1979 To 2014) were first transformed into wind stress based on [S26]:

$$(\tau_x,\tau_y) = 10^{-3}\rho_a(0.142U+0.076U^2+2.7)(u_a,v_a), \quad \text{(S18)}$$

where $\rho_a = 1.25$ kg m^{-3} is the air density, U is the wind speed, and u_a, v_a are zonal and meridional wind components. Then, we assume, based on the data, that the auto-correlation function of the wind stress components follows:

$$\langle\tau_{x,y}(\tilde{t})\tau_{x,y}(\tilde{t}+t)\rangle = \frac{1}{2}\tau_{x,y_0}\cos(\omega_0 t) + \frac{1}{2}\tau_{x,y_0}e^{-\gamma_{x,y}|t|}, \quad \text{(S19)}$$

where ω_0 is the diurnal frequency. [We have estimated the KE based on the power spectrum of the wind stress and by directly numerically integrating Eq. (6) and obtained results that are very similar to the results described below. The advantage of using the present approach is the ability to estimate the contribution of the different components of the wind stress.] We first estimate τ_{x,y_0} from the FT of $\tau_{x,y}$, then find τ_{x,y_1} from Eq. (S19) at lag $t = 0$, then estimate the exponents $\gamma_{x,y}$ from the auto-correlation function of the first lags.

The estimated exponents, $\gamma_{x,y}$, are shown in Fig. S2 and the two exhibit similar pattern. Generally speaking, the low latitudes (30°S to 30°N) are more correlated than the higher latitudes that are weakly correlated in regions of enhanced storm activity (e.g., the storm tracks and high mountains). The mean values of the exponents over the ocean are very similar to the mean value over the land and are $\langle\gamma_x\rangle = 10^{-5}$ s^{-1}, $\langle\gamma_y\rangle = 1.2\times10^{-5}$ s^{-1}.

The different components of the wind stress are shown in Fig. S3. The correlated noise component, τ_1 (Fig. S3a), is high at the regions of enhanced wind activity like the storm track and high mountains and it roughly matches the regions of high correlation exponents $\gamma_{x,y}$ shown in Fig. S2. τ_1 is larger than the periodic wind component τ_0 (Fig. S3b) by more than an order of magnitude. The periodic component is often large in regions of large noise component, indicating that the periodicity is in part due to higher wind energy (power) in these regions. The mean wind-stress component, τ_m, is high only in the southern ocean and along the edge of Antarctica. The global mean values of τ_1, τ_0, τ_m over the ocean is 0.26, 6.6×10^{-3}, 0.075 N m^{-2} respectively and is very similar to the wind-stress values over land.

Given the wind-stress components, $\tau_{x,y_{0,1,m}}$ it is possible to calculate the KE that is associated with each of the components, based on the ocean depth at each grid point and based on Eqs. (5), (7). The KE of the entire water column is shown in Fig. S4. The KE that is associated with temporal correlation, $E_{k,1}$, and is much larger than the two other components associated with the diurnal periodicity, $E_{k,0}$, and the mean wind stress, $E_{k,m}$. The global mean of the three components of the KE is $E_{k,1} = 7.27\times10^{17}$J, $E_{k,0} = 1.4\times10^{17}$J and $E_{k,m} = 6.44\times10^{15}$J. While $E_{k,1}$ is significant in vast ocean regions, $E_{k,0}$ is very strong, as expected, around latitude 30°. The estimated KE is obviously not realistic as it ignores all spatial dynamics and is about 1/5 of realistic estimation of global ocean KE $\sim 5.2\times10^{18}$J [S27]. The most important parameter is the viscosity coefficient which was chosen to be 0.1 m^2 s^{-1}; it is reasonable that ν is much smaller at depth where the eddy activity is weaker (similar to effect of weak stratification on the diffusion coefficient, [S22]) such that the resultant currents will be stronger leading to larger KE.

We have also calculated the KE of the deep ocean (deeper than 1 km) and find that significant part is stored in the deep ocean. Fig. S5 depicts the ratio, r, between the deep ocean KE and the global KE and, consisting with our predictions, the stochastic (Fig. S5a) and periodic (Fig. S5b) components of the wind stress account for tens of percents of total KE. The deep ocean KE that resulted from the mean forcing (Fig. S5c) is, as expected, negligible. Specifically, the global mean deep ocean KE is $E_{k,1}(H > 1\text{km}) = 2.49\times10^{17}$J ($r_1 = 34\%$), $E_{k,0}(H > 1\text{km}) = 6.04\times10^{16}$J ($r_0 = 44\%$) and $E_{k,m}(H > 1\text{km}) = 2.4\times10^{12}$J ($r_m = 0.04\%$). The ratio captures the pattern of the deep ridges as the KE depends on ocean depth H.

The above calculations were based on the assumption that the ocean is strongly stratified. However, the deep ocean is only weekly stratified such that one expects weaker currents and KE (see Fig. S1 of the main text). MITgcm simulations with open boundary restoring of temperature and salinity of the global and temporal mean of Levitus atlas [S28] resulted in linearly decreasing current speed in the few upper kms of the ocean and almost uniform current speed in the abyssal ocean. However, the eddy viscosity coefficient may be smaller under such conditions due to the weaker eddy activity, probably leading to stronger currents and hence larger KE. Thus, the values given above only very roughly estimate the ocean's KE.

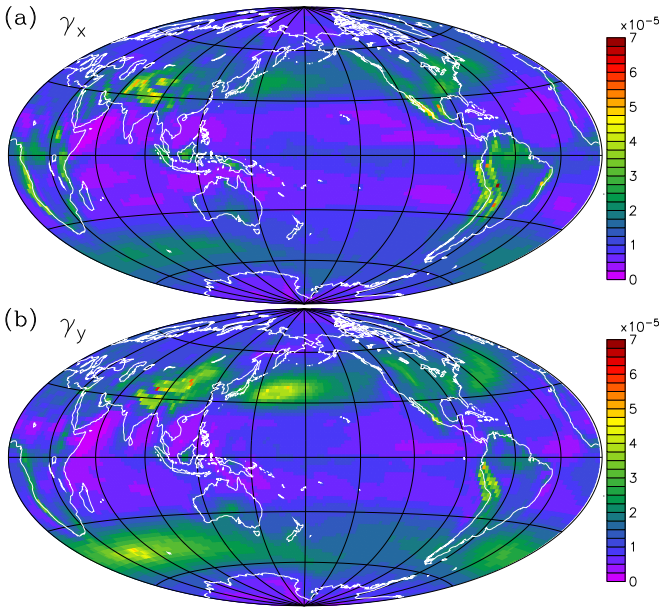

FIG. S2: Temporal correlation exponent, (a) γ_x and (b) γ_y, in s^{-1}, estimated based on NCEP reanalysis 2 surface (10 m) winds.

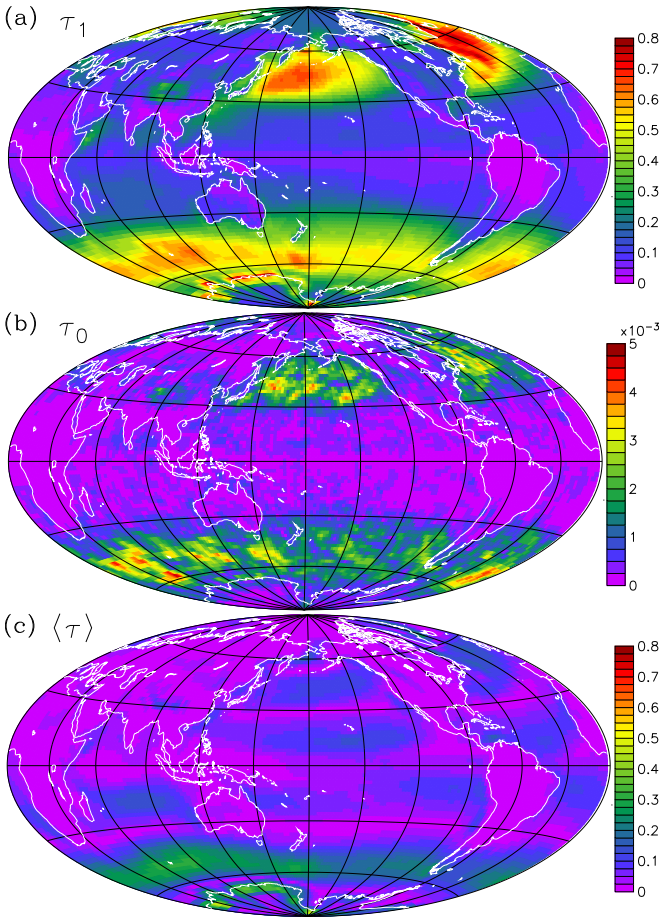

FIG. S3: Wind-stress coefficient (in N m^{-2}) of the (a) stochastic, $\tau_1 = \sqrt{\tau_{x,1}^2 + \tau_{y,1}^2}$, (b) periodic, $\tau_0 = \sqrt{\tau_{x,0}^2 + \tau_{y,0}^2}$, and (c) mean, $\tau_m = \sqrt{\langle \tau_x \rangle^2 + \langle \tau_y \rangle^2}$, components of the wind stress. Estimated based on NCEP reanalysis 2 surface (10 m) winds.

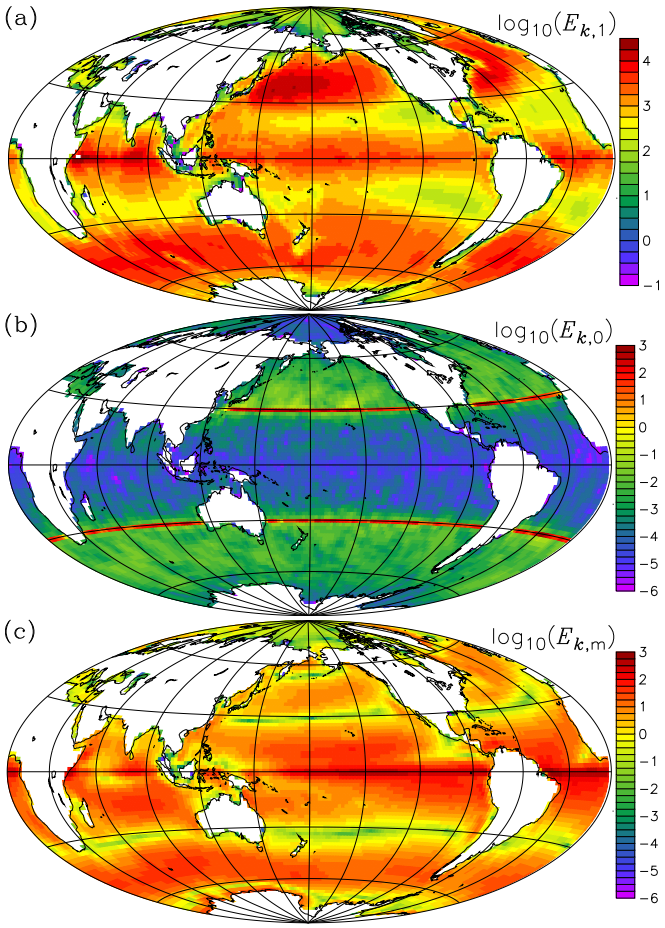

FIG. S4: KE wind-stress coefficient (in N m^{-2}) of the (a) stochastic, τ_1, (b) periodic, τ_0, and (c) mean, τ_m, components of the wind stress. Estimated based on NCEP reanalysis 2 surface (10 m) winds.

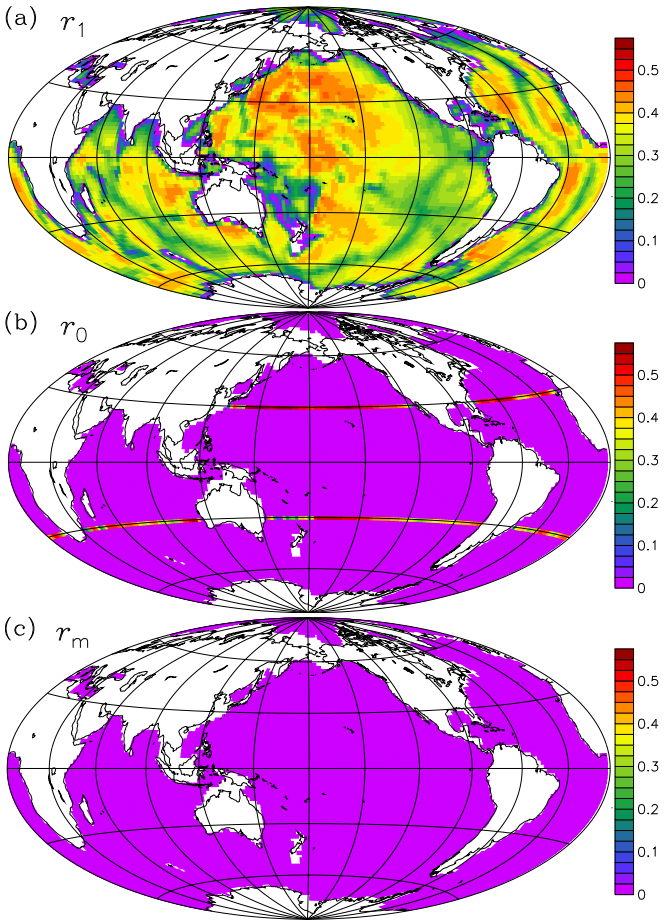

FIG. S5: Ratio between the KE of the deep ocean (deeper than 1 km) and entire water column KE for the (a) stochastic, (b) periodic, and (c) mean components of the wind stress. Estimated based on NCEP reanalysis 2 surface (10 m) winds and numerical integration of Eq. (6).